

University of Groningen

Homozygous whole body Cbs knockout in adult mice features minimal pathology during ageing despite severe homocysteinemia

Nakladal, D; Lambooy, S P H; Mišúth, S; Čepcová, D; Joschko, C P; van Buiten, A; Goris, M; Hoogstra-Berends, F; Kloosterhuis, N J; Huijkman, N

Published in:
The FASEB Journal

DOI:
[10.1096/fj.202101550R](https://doi.org/10.1096/fj.202101550R)

IMPORTANT NOTE: You are advised to consult the publisher's version (publisher's PDF) if you wish to cite from it. Please check the document version below.

Document Version
Publisher's PDF, also known as Version of record

Publication date:
2022

[Link to publication in University of Groningen/UMCG research database](#)

Citation for published version (APA):

Nakladal, D., Lambooy, S. P. H., Mišúth, S., Čepcová, D., Joschko, C. P., van Buiten, A., Goris, M., Hoogstra-Berends, F., Kloosterhuis, N. J., Huijkman, N., van de Sluis, B., Diercks, G. F., Buikema, J. H., Henning, R. H., & Deelman, L. E. (2022). Homozygous whole body Cbs knockout in adult mice features minimal pathology during ageing despite severe homocysteinemia. *The FASEB Journal*, 36(4), [22260]. <https://doi.org/10.1096/fj.202101550R>

Copyright

Other than for strictly personal use, it is not permitted to download or to forward/distribute the text or part of it without the consent of the author(s) and/or copyright holder(s), unless the work is under an open content license (like Creative Commons).

The publication may also be distributed here under the terms of Article 25fa of the Dutch Copyright Act, indicated by the "Taverne" license. More information can be found on the University of Groningen website: <https://www.rug.nl/library/open-access/self-archiving-pure/taverne-amendment>.


Take-down policy

If you believe that this document breaches copyright please contact us providing details, and we will remove access to the work immediately and investigate your claim.

Downloaded from the University of Groningen/UMCG research database (Pure): <http://www.rug.nl/research/portal>. For technical reasons the number of authors shown on this cover page is limited to 10 maximum.

RESEARCH ARTICLE

Homozygous whole body *Cbs* knockout in adult mice features minimal pathology during ageing despite severe homocysteinemia

D. Nakladal¹  | S. P. H. Lambooy¹ | S. Mišúth^{1,2} | D. Čepcová^{1,2} | C. P. Joschko¹ | A. van Buiten¹ | M. Goris¹ | F. Hoogstra-Berends¹ | N. J. Kloosterhuis³ | N. Huijckman⁴ | B. van de Sluis^{3,4} | G. F. Diercks⁵ | J. H. Buikema¹ | R. H. Henning¹ | L. E. Deelman¹

¹Department of Clinical Pharmacy and Pharmacology, University of Groningen, University Medical Center Groningen, Groningen, The Netherlands

²Department of Pharmacology & Toxicology, Faculty of Pharmacy, Comenius University in Bratislava, Bratislava, Slovakia

³Department of Pediatrics, University of Groningen, University Medical Center Groningen, Groningen, The Netherlands

⁴iPSC/CRISPR Center Groningen, University of Groningen, University Medical Center Groningen, Groningen, The Netherlands

⁵Department of Dermatology, Center for Blistering Diseases, University of Groningen, University Medical Center Groningen, Groningen, The Netherlands

Correspondence

D. Nakladal, Department of Clinical Pharmacy and Pharmacology, AP50, University Medical Center Groningen (UMCG), Hanzeplein 1, PO BOX 30001, 9700 RB Groningen, The Netherlands.
Email: d.nakladal@umcg.nl

L. E. Deelman, Department of Clinical Pharmacy and Pharmacology, AP50, University Medical Center Groningen (UMCG), Hanzeplein 1, PO BOX 30001, 9700 RB Groningen, The Netherlands.
Email: l.e.deelman@umcg.nl

Funding information

DN was financially supported by an Abel Tasman PhD scholarship by the Graduate School of Medical Sciences, University of Groningen, University Medical Center Groningen and by Life Sciences and Health—Topconsortium voor Kennis en Innovatie (Stichting LSH-TKI): PPP project-2019-017

Abstract

Deficiencies in Cystathionine- β -synthase (CBS) lead to hyperhomocysteinemia (HHCy), which is considered a risk factor for cardiovascular, bone and neurological disease. Moreover, CBS is important for the production of cysteine, hydrogen sulfide (H_2S) and glutathione. Studying the biological role of CBS in adult mice has been severely hampered by embryological disturbances and perinatal mortality. To overcome these issues and assess the effects of whole-body CBS deficiency in adult mice, we engineered and characterized a Cre-inducible *Cbs* knockout model during ageing. No perinatal mortality occurred before *Cbs*^{-/-} induction at 10 weeks of age. Mice were followed until 90 weeks of age and ablation of *Cbs* was confirmed in liver and kidney but not in brain. Severe HHCy was observed in *Cbs*^{-/-} ($289 \pm 58 \mu M$) but not in *Cbs*^{+/-} or control mice ($<10 \mu M$). *Cbs*^{-/-} showed impaired growth, facial alopecia, endothelial dysfunction in absence of increased mortality, and signs of liver or kidney damage. CBS expression in skin localized to sebaceous glands and epidermis, suggesting local effects of *Cbs*^{-/-} on alopecia. *Cbs*^{-/-} showed increased markers of oxidative stress and senescence but expression of other H_2S producing enzymes (CSE and 3-MST) was not affected. CBS

Abbreviations: 3-MST, 3-mercaptopyruvate sulfurtransferase; BAC, bacterial artificial chromosome; CSE, cystathionine gamma-lyase; Hcy, homocysteine; HHCy, hyperhomocysteinuria; HHCy, hyperhomocysteinemia; NASH, Non-alcoholic steatohepatitis; PAS, periodic acid-Schiff staining; tHcy, total (plasma) homocysteine.

This is an open access article under the terms of the Creative Commons Attribution License, which permits use, distribution and reproduction in any medium, provided the original work is properly cited.

© 2022 The Authors. *The FASEB Journal* published by Wiley Periodicals LLC on behalf of Federation of American Societies for Experimental Biology

deficiency severely impaired H₂S production capacity in liver, but not in brain or kidney. In summary, *Cbs*^{-/-} mice presented a mild phenotype without mortality despite severe HHCy. The findings demonstrate that HHCy is not directly linked to development of end organ damage.

KEYWORDS

cystathionine beta synthase deficiency, hydrogen sulfide, hyperhomocysteinemia, inducible mouse model, vascular dysfunction

1 | INTRODUCTION

Elevated plasma levels of the amino acid homocysteine (hyperhomocysteinemia or HHCy) is an overarching risk factor for cardiovascular disease, chronic kidney disease and Alzheimer's disease.¹⁻⁴ In HHCy, plasma concentration of Hcy can increase 10- to 20-fold, reaching levels as high as 200–300 μM. Although HHCy is an established risk factor, the pathogenic consequences of HHCy in disease etiology and the underlying molecular pathways are still under debate.⁵ There is evidence that high homocysteine levels can induce the formation of ROS via increased *P66shc* expression,⁶ which negatively affects endothelial function. More specifically, it has been suggested that HHCy may cause endothelial dysfunction by activating protein kinase C (PKC) and reducing nitric oxide (NO) production by eNOS in C57BL/6 *Cbs*^{-/-} mice.⁷ In addition, HHCy also affects many other up- and downstream effectors such as SAM, SAH, cystathionine, total cysteine (tCys), glutathione (GSH) and hydrogen sulphide (H₂S).⁸ However, total Hcy remained the best predictor for clinical severity.⁸

Plasma homocysteine levels are largely governed by the methionine and transsulfuration pathways, which are responsible for the metabolic conversion of homocysteine to the amino acids cystathionine and cysteine. Therefore, disturbances and/or deficiencies in either pathway may result in HHCy. Mild cases of HHCy may be caused by disorders such as impaired vitamin B12 uptake.⁹ More severe cases of HHCy are frequently associated with genetic defects in the gene for cystathionine-β-synthase (CBS) with an incidence of approximately 1 in 100 000 in western countries.¹⁰

CBS is a lyase-class enzyme that is predominantly expressed in the liver and kidney and is pivotal in the transsulfuration pathway mainly for its catalytic condensation of homocysteine (Hcy) with serine to form cystathionine. Due to its relaxed substrate specificity, it also can produce the gasotransmitter H₂S in a reaction between cysteine and homocysteine. H₂S is a gasotransmitter produced in the transsulfuration pathway and is

highly reactive, and therefore involved in a wide range of biological processes. Specifically, H₂S is regarded as a component of the endothelium-derived hyperpolarizing factor (EDHF), which is important for maintenance of arterial relaxation.¹¹ Additionally, H₂S was found to mitigate both heart failure in patients and kidney disease in obese mice, and has been implicated to promote longevity.¹²⁻¹⁴ Recently, the effects of H₂S were highlighted in mitochondria, opening a new avenue of regulatory mechanisms.¹⁵

To investigate the complicated molecular mechanisms of HHCy, several mouse models of CBS deficiency have been developed. Among the first is the Maeda model in which homozygous *Cbs* knockout mice proved notoriously difficult to breed.¹⁶ The mendelian inheritance of *Cbs*^{-/-} was found in 23%–50% less C57/BL6 mice than expected, and postnatal mortality was approximately 90% within the first five weeks.¹⁶ The cause of neonatal mortality in *Cbs*^{-/-} mice was attributed to liver failure from severe fibrosis and neutrophil infiltration. In surviving *Cbs*^{-/-} mice, liver damage was observed in the form of increased ALAT and AST activities,¹⁷ steatotic hepatomegaly, and early fibrosis with elevated levels of TNF-α and IL-6.¹⁸ The Maeda knockout allele has also been crossed into C57/BL6J, BABL/cA, C3H/HeJ and DBA/2J, of which the C3H/HeJ had the highest survival rate (30.8%), and variable tHcy levels did not seem to play a role in survival.¹⁹ To prevent high death rates, a *Tg-hCBS Cbs*^{-/-} mouse model was developed, in which a human CBS gene under the control of a zinc sensitive promoter was introduced, enabling rescue of embryonic *Cbs*^{-/-} mice by the addition of zinc to the drinking water.²⁰ The *Tg-hCBS Cbs*^{-/-} mouse carrying the I278T mutation showed less liver damage despite tHcy levels that were elevated while still on zinc-laced water. This model had an expected Mendelian birth ratio and the same survival rates as heterozygotes. In addition, the HO (human only) *Cbs* knockout mouse was generated by first injecting the complete human CBS gene that was included in a bacterial artificial chromosome (BAC) into the germ line followed by crossing with the Maeda

TABLE 1 Animals used in the study were grouped based on injection of tamoxifen or vehicle control (corn oil), *Cbs* genotype and *Cre* genotype

Group	<i>Cbs</i> ^{fl/fl}	<i>Cbs</i> ^{-/-}	<i>Cbs</i> ^{+/fl}	<i>Cbs</i> ^{+/-}	<i>Cbs</i> ^{fl/fl} + C	<i>Cbs</i> ^{fl/fl} + T
Injection	Corn oil	Tamoxifen	Corn oil	Tamoxifen	Corn oil	Tamoxifen
<i>Cbs</i> genotype	Homozygous	Homozygous	Heterozygous	Heterozygous	Homozygous	Homozygous
<i>Cre</i> genotype	Heterozygous	Heterozygous	Heterozygous	Heterozygous	Wild-type	Wild-type

knockout mouse.²¹ HO *Cbs* knockout mice lacked neonatal lethality, did not suffer from hepatic steatosis, had mildly increased ALAT levels and showed residual CBS activity with—for unknown reasons—quite variable plasma homocysteine concentrations.

Human CBS deficiency is often accompanied by Marfan syndrome which features low BMI and body fat.²² Consistent with this fact, fat mass but not lean mass was reduced in *Tg-I278T Cbs*^{-/-} mice.²³ Endothelial dysfunction was showcased in the mesenteric artery of *Tg-hCBS Cbs*^{-/-} mice, caused by HHCy-induced oxidative stress impairing NO- and EDHF-mediated relaxation.²⁴ In this study, endothelium-independent (SNP) and prostacyclin-mediated relaxations were not affected by CBS deficiency. Additionally, mice with severe HHCy reportedly developed endothelial dysfunction in cerebral arteries with SNP relaxation unaffected by HHCy.²⁵ Similar to human CBS deficiency, non-transgenic *Cbs*^{-/-} and *Tg-I278T Cbs*^{-/-} mice exhibited facial alopecia which was a result of epidermal hyperkeratosis, dermal layer thinning and decreased hair diameter, and was reversible by low methionine diet.²⁶

Although these models have been helpful to initially understand the role of CBS and HHCy in disease development, it is unclear if these models reflect natural CBS deficiency as both the *Tg-hCBS* and HO *Cbs* knockout models depend on expression of transgenic (human) CBS to overcome perinatal mortality. In addition, the requirement for stimulation of a zinc-inducible metallothionein promoter^{20,23} may not necessarily mimic natural CBS localization. The expression of a human CBS transgene in mice may therefore have profound effects on the endogenous regulation of the methylation and transsulfuration pathways and limit the relevance of these models for studying the role of CBS and HHCy in disease development.

To overcome these problems, we developed a conditional *Cbs* knockout mouse model based on the *Cre/LoxP* recombination system that is inducible by tamoxifen. The purpose of this model is to facilitate and improve our understanding of the role of CBS and HHCy in disease development. For this, we investigated the long-term general, organ, and vascular phenotype of tamoxifen/*Cre*-induced *Cbs*^{-/-} and *Cbs*^{+/+} mice up until 80 weeks of age.

2 | MATERIALS AND METHODS

2.1 | Animal care and experimental protocol

Experiments were approved by the Institutional Animal Care and Use Committee of the University of Groningen, The Netherlands and by the Central Committee for Animal Testing with approval number 16427-02-01. Further, all methods were performed in accordance with the relevant guidelines and regulations. Mice were housed solitarily and maintained in an ambient temperature (21°C) controlled environment with 12 h/12 h light/dark cycle and ad libitum access to standard chow and water (801151, RM1 maintenance, Special Diets Services). A total of 25 males and 23 females were deployed for the study, which were evenly distributed into six groups based on treatment and genotype (Table 1). At an average age of 10 weeks, half the mice received tamoxifen while the other mice were mock injected with corn-oil. *Cbs* was knocked out by *Cre* recombinase induced by repeated daily tamoxifen injections (75 mg/kg body weight, i.p.) for 5 consecutive days. Animals were weighed every other week and at the age of 52, and 75 weeks, mice were placed in metabolic cages for 24 h. Urine was collected and metabolic parameters were recorded, including water intake, urine output and body weight. Prior to termination, the percentage of body weight composed of adipose tissue was dissected using nuclear magnetic resonance. Mice were briefly restrained without anesthesia and placed in a minispec LF Series (Bruker, Billerica, MA, USA), where fat tissue, lean tissue and free fluid composition were measured. In addition, mean arterial blood pressure was measured in conscious mice by means of the tail-cuff method (PS-200A; Riken-Kaihatsu; Tokyo, Japan). At the age of 90 weeks, anesthesia was induced in mice by inhalation of 5% isoflurane in oxygen, and mice were humanely terminated by exsanguination. Samples of blood were collected in EDTA tubes, and organs were harvested and split for storage in liquid nitrogen and 4% buffered formaldehyde for fixation (50-00-0 Klinipath—VWR, Amsterdam, The Netherlands).

2.2 | Generating a conditional *Cbs* knockout mouse model

A *Cbs* targeting construct in which exon 3 of *Cbs* was flanked by loxP recombination sites preceded by a neomycin selection cassette under the control of a PGK and EM7 promoter and trailed by the bGH polyadenylation sequence (bGHpA) was generated using a method described previously²⁷ (Figure 1A). The entire construct was sequenced to verify correct assembly. The targeting vector was electroporated into 129/SvEv embryonic stem (ES) cells and screened for homologous recombination by Southern blotting. Three clones positive for homologous recombination were amplified and used to generate chimeric mice. Chimeric mice were produced by microinjection of ES cell targeted clones into C57BL/6 blastocysts. Chimeric males were crossed with C57BL/6 females and these chimeras successfully transmitted the floxed allele. F1 heterozygote mice derived from each clone were crossed with Flp germ-line deleter strain

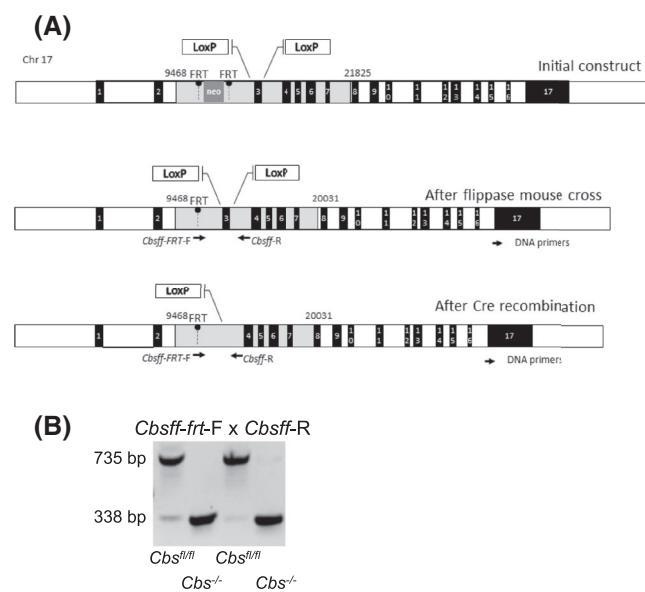


FIGURE 1 Genetic engineering and genotyping of tamoxifen-induced *Cbs* knockout mouse. (A) Top: diagram showing the *Cbs* targeting construct with exon 3 of *Cbs* flanked by loxP recombination sites. In addition, the construct contained a neomycin selection cassette flanked by short flippase (Flp) recognition target sites (FRT) inserted in intron 2. Middle: the neomycin selection cassette was subsequently removed by selective breeding in Flp mice, leaving one FRT site intact. Bottom: Tamoxifen-induced Cre-mediated excision of exon 3 can be detected by PCR using primers *Cbsff-FRT-F* and *Cbsff-R*. (B) Confirmation of tamoxifen-induced Cre-mediated excision of exon 3 using PCR and gel electrophoresis in liver DNA from *Cbs*^{fl/fl} obtained two weeks after induction. Predominantly intact construct (735 bp) was detected in controls treated with corn oil whereas nearly completely Cre-mediated excision (338) was achieved in mice treated with tamoxifen

(FLPe deleter strain (B6;SJL-Tg(ACTFLPe)9205Dym/J, Strain #003800; The Jackson Laboratory, Bar Harbor, Me, USA) to remove the neomycin selection cassette and generate *Cbs*^{flx/flx} mice (Figure 1A, Table 1), which were kept on a mixed 129/SvEv × C57BL/6 genetic background. The mice were crossed with C57BL/6 harboring the Cre-ERT2 transgene (B6.129-Gt(ROSA)26Sor^{tm1(cre/ERT2)Tyj}/J, Strain #008463, The Jackson Laboratory, Bar Harbor, Me, USA), a kind gift from Dr. Floris Fojjer. The ROSA26 locus which is generally used for constitutive, ubiquitous gene expression in mice was driving Cre-ERT2 as described previously.²⁸ The resulting conditional *Cbs* knockout mouse model was maintained on a mixed 129/SvEv × C57BL/6 genetic background.

2.3 | Quantification of facial alopecia

To determine the severity of facial alopecia, hair loss was assessed at six skin locations (snout, side of head, top of head, cheeks, whiskers, and neck) using a 3-point score for hair loss (0; no loss, 1; light, 2; moderate, 3; severe/complete). A composite alopecia score was subsequently determined by calculating the sum of all scores (min, 0; max; 18).

2.4 | Plasma homocysteine and H₂O₂ measurement

After collection of blood in 1.5 ml EDTA tubes, samples were centrifuged at 2000 g for 10 min at 4°C and the supernatant was collected, snap frozen in liquid nitrogen and stored at -80°C. Total homocysteine (tHCy) levels were determined on an Architect system (Abbott, Netherlands) using a Homocysteine Reagent Kit (ABBL482R02, Abbott, Netherlands). Plasma samples were diluted 25-fold to achieve the required 250 μl sample volume. Plasma homocysteine levels in control groups fell below the lower limit of detection (LLOQ, 1 μM). Given that concentrations of tHCy levels in diluted samples of control groups were below plasma tHCy levels before dilution could not have exceeded 25 μM. To establish the average tHCy levels in control groups, samples were pooled and reassessed at a 4-fold dilution. Plasma hydrogen peroxide levels were determined using an Amplex Red H₂O₂ kit, Life Technologies (A22188), Leusden, The Netherlands.

2.5 | Urinary measurements

Urinary albumin levels were determined with a mouse Albumin Elisa kit (ab108792, Abcam, Cambridge, UK).

Urinary creatinine was measured with the Creatinine (urinary) Colorimetric Assay Kit (500701, Cayman Chemical, Ann Arbor, USA).

2.6 | Real-time qPCR

RNA from liver, kidney, and brain were isolated using an RNA isolation kit (NucleoSpin, RNA II, Macherey-Nagel). Integrity of RNA was validated using agarose gel electrophoresis. RNA concentrations were measured spectrophotometrically at 260 nM. Subsequently, RNA (1 µg) was reversely transcribed into cDNA. Real-Time PCR was performed using Absolute™ qPCR SYBR® Green ROX Mix (Westburg, Leusden, The Netherlands), 400 nM of primer and 2.5 µl template DNA in a total volume of 25 µl. Temperature profiles were set to 95°C for 15 min followed by 40 cycles of denaturing at 95°C for 15 s and annealing/extending at 60°C for 1 min. Primers used for cDNA quantification were *GAPDH* (forward 5'-GCAAATTCACGGCACAG-3', reverse 5'-CACCAGTAGACTCCACGAC-3'), *MnSOD* (forward 5'-ACAACCTCAGGTCGCTCTTCA-3', reverse 5'-TGATAGCCTCCAGCAACTCT-3'), *P16* (forward 5'-TCGTACCCGATACAGGTGAT-3', reverse 5'-GAGCTGCCACTTTGACGTTG-3'), and *LMNB1* (forward 5'-GGGAAGTTTATTCGCTTGAAGA-3', reverse 5'-ATCTCCCAGCCTCCCATT-3').

2.7 | Genotyping

Mice DNA was extracted from ear punches by full digestion in 100 µl buffer (50 mM KCl, 10 mM Tris, 0.1% Triton X-100, 0.4 mg/ml Proteinase K; pH 8.0). 2 µl of DNA extract was added to 12.7 µl of Master Mix (GoTaq, Promega, Leiden, The Netherlands) and 0.3 µl of primers (final concentration 0.3 µM), using a PCR protocol comprising 95°C for 3 min, followed by 35 cycles of 95°C denaturation for 35 s, 50 s annealing at 59°C, elongation at 72°C for 45 s, followed by a 3 min 72°C elongation step. Primers used for DNA genotyping were *Cbs^{fl/fl}*-F (forward 5'-CGACGCCAGTGAATTGTAATACG-3'), *Cbs^{fl/fl}*-R (reverse TGCTTGCTCTGATAGCTCCACTTC), designed to produce a 735 bp band in *Cbs^{fl/fl}* mice and a 338 bp product following tamoxifen treatment in *Cbs^{-/-}* mice.

2.8 | SDS-page immunoblotting

Samples of liver, kidney and brain tissue were homogenized in ice-cold RIPA solution (Igepal ca-630, sodium deoxycholate and 20% sodium dodecyl sulfate (SDS) in PBS) enriched

with protease inhibitor cocktail (11836170001, Roche Diagnostics, Almere, The Netherlands), sodium orthovanadate (S6508, Sigma-Aldrich) and β-mercaptoethanol (805740, Sigma-Aldrich). Total protein concentration was determined using Bradford assay (5000116, Bio-Rad Laboratories, Veenendaal, The Netherlands) and 25 µg protein in 25 µl per sample was loaded onto a commercial gel (4568093, Bio-Rad). Proteins were separated by electrophoresis and transferred onto a nitrocellulose membrane using Trans-Blot Turbo System (1620115 and 10026938 respectively, Bio-Rad Laboratories). Free nitrocellulose sites were blocked with 5% skim milk (70166, Sigma-Aldrich, Zwijndrecht, The Netherlands) for 20 min and membranes were incubated overnight at 4°C with either anti-CBS antibody (1:1000 dilution, D8F2P, Cell Signaling Technology, Danvers, MA, USA), anti-CSE antibody (1:1000 dilution, ab151769, Abcam), or anti-3-MST antibody (1:1000 dilution, HPA001240, Sigma-Aldrich) in 3% BSA. After three subsequent washes with TBST, membranes were incubated with secondary Goat Anti-Rabbit antibody conjugated with HRP (1:2000, P0448, Dako) at RT for 2 h. Chemiluminescent signal was detected using Western Lightning Ultra (NEL112001EA, Perkin Elmer International, Groningen, The Netherlands). Chemiluminescent signal was normalized to total lane protein volume using the standard BioRad StainFree TGX blot technology.

2.9 | Mulvany myography of the mouse aorta

During the termination procedure, thoracic aorta and surrounding adipose tissue were surgically removed and placed in cold saline solution (0.9% NaCl, 4°C). Aortas were carefully dissected from perivascular adipose tissue and cut into 2 mm long rings using a Leica S4E stereoscopic microscope, Vannas stainless steel Curved Spring Scissors with 3 mm Blades and Dumont #5 Medical Biology Forceps. Aortic rings were mounted on pins (ø = 200 µm) in a Mulvany Multi Wire Myograph system model 610 M (Danish Myo Technology, Aarhus, Denmark) and incubated at 37°C in organ baths filled with 5 ml normal physiological Krebs buffer (pH 7.4). Isometric force was sampled, analogue signal was transformed to digital signal using PowerLab 8/30 (ADInstruments) and a myogram was recorded in PowerLab Chart v 5.3. After 20 min of equilibration, aortic rings were stretched to transmural pressure of 13.3 kPa using the proprietary DMT Normalization Procedure software module. Initially, aortic rings were subjected to two subsequent wake-up protocols: addition of 60 mM KCl (7447-40-7, Merck, Schiphol-Rijk, The Netherlands), stabilization of the response, three times wash-out, and equilibration.

Endothelium-dependent relaxation (EDR) was assessed in aortic rings pre-constricted with phenylephrine (PE, 1 μ M) and endothelial relaxation responses were recorded in response to cumulative additions of acetylcholine (100 nM–100 μ M, A6625, Sigma-Aldrich). For this experiment, rings from all groups were pre-incubated for 20 min after an addition of physiological saline solution as vehicle control, while in groups *Cbs*^{-/-} and *Cbs*^{fl/fl} additional rings were pre-incubated with 100 μ M L-NMMA (53308-83-1, Zwijndrecht, Netherlands).

2.10 | Histology and morphological analysis

During the termination procedure after the animals were killed, organs were immediately placed in cold saline solution, portioned, and fixated in 4% formaldehyde solution for several days. After embedding in paraffin, 4 μ m thick sections were cut (HistoCore AUTOCUT, Leica) and placed on 76 \times 26 mm glass slides (Starfrost, Brunswick, Germany).

2.10.1 | Hematoxylin and Eosin staining

Liver and kidney sections were deparaffinized and hydrated using an ethanol gradient (100%, 96%, and 70%, 10 min each). Sections were suspended in Mayer's hematoxylin (5 min, MHS32, Sigma), washed with tap water, and incubated in an eosin solution (5 min) and washed again. Sections were dehydrated and fixed in the DePeX mounting resin (18243.01, Serva, VWR, Netherlands). Kidney sections stained with Hematoxylin and Eosin (HE) were examined at 20 \times magnification for foci of tubulointerstitial fibrosis and graded using a scale from 0 to 4 (0—normal; 1—involvement of <10% of the cortex; 2—involvement of 10%–25% of the cortex; 3—involvement of 25%–75% of the cortex; and 4—extensive damage involving >75% of the cortex). Tubular injury was determined using 5 random non-overlapping fields of renal cortex at 20 \times magnification, and tubular dilatation and tubular necrosis were also assessed. For tubular dilatation, the scores were assigned in the following manner: 0 = absence, 1 = <5 dilated cortical tubules observed per field, 2 = 5–10 dilated cortical tubules observed per field, 3 = 10< dilated tubules observed per field. Tubular necrosis was graded on a scale from 0 to 4 as described previously.²⁹ For glomerulosclerosis, the first 3 randomly selected glomeruli at the kidney cortex were examined and graded. The sections were scored as follows: 0 = normal, 1 = <25% involvement, 2 = <50% involvement, 3 = <75%, and 4 = 75%< sclerosis, and the average of 3 individual scores was calculated to generate the glomerulosclerosis score.

2.10.2 | Periodic acid Schiff staining

Liver sections were deparaffinized in two subsequent incubations in xylene for 10 min each, and hydrated. Sections were incubated in 0.5% periodic acid solution (101646/1, Merck, Netherlands) for 10 min, rinsed with water, and incubated in Schiff's reagent (101646/2, Merck) for 30 min. Samples rinsed with water were counterstained in Mayer's hematoxylin, dehydrated, and fixed in DePeX mounting resin. The intensity of glycogen staining in liver sections was quantified using ImageJ software setting the lower and upper thresholds to 0 and 128 respectively, and the staining intensity (% area) was recorded for each image.

2.10.3 | Oil Red O staining

Liver cryosections (10 μ m) mounted on glass slides were dried for 60 min and fixed in ice cold 4% formalin for 5 min and rinsed 3 times with demineralized water. Slides were first placed in absolute propylene glycol for 3.5 min and then directly into Oil Red O (ORO) solution prewarmed to 60°C for 10 min. Samples were differentiated in 85% propylene glycol solution for 4 min. After rinsing with demineralized water, slides were mounted using aqueous Faramount medium (S3025 Agilent-Dako, Santa Clara, CA, United States). Oil red O staining was quantified using ImageJ software by setting the lower and upper thresholds to 60 and 135 respectively, and the staining intensity (% area) was recorded for each image.

2.10.4 | CBS staining

Liver, kidney, and skin sections were deparaffinized and hydrated. Heat-induced epitope retrieval was performed overnight at 60°C in citrate buffer pH = 6 (S1804, Sigma). The coupes were allowed to cool to room temperature and were washed twice with PBS buffer (4391.9010, Klinipath, Duiven, Netherlands). Endogenous peroxidases were blocked with 0.3% hydrogen peroxide (822287, Sigma-Aldrich) for 30 min. After two subsequent washes with PBS, sections were blocked with 10% goat serum in 1% BSA for 30 min (X0907, Agilent-Dako). Blocking was followed with overnight incubation at 4°C with the primary rabbit anti-CBS antibodies (1:200 dilution, D8F2P, Cell Signaling, for liver and skin sections), and (1:5000 dilution, 14787-1-AP, proteintech, for kidney sections), in PBS with 1% goat serum and 1% BSA. After three washes with PBS, secondary HRP-conjugated goat anti-rabbit antibody (1:100 dilution, P01447, DAKO in PBS with 1% BSA) was incubated for 1 h at room temperature. The slides were washed twice with PBS, DAB chromogen (ab64238, Abcam) was used for 10 min to develop brown staining and stopped with tap water. Nuclei were counterstained with hematoxylin for 30 s and rinsed tap

water. Sections were then dehydrated using ethanol (70%, 96%, 100%), air-dried, and mounted with DePeX.

2.11 | Measurement of H₂S production

Tissue was scraped on dry ice and homogenized using an overhead stirrer at 750RPM (VOS40 digital, VWR, Amsterdam, The Netherlands) in cold Milli-Q[®] ultrapure water to prepare a 10% (w/v) homogenate. The assay reaction mix was formulated to 10 μ l volume on a Hard-Shell[®] 384-Well PCR Plate (HSP3841, BioRad, Lunteren, The Netherlands), and contained 0.1 M Hepes buffer (pH 7.4), 0.25 mM pyridoxal-5-phosphate (PLP), 2 mM homocysteine, 10 mM cysteine and 1 μ l of liver lysate. To detect H₂S gas escaping from the liquid phase, we used MN 710 Grade Filter Papers (150047A, Macherey-Nagel[™]/Fisher Scientific, Landsmeer, The Netherlands) cut to the dimensions of a 384-well plate, soaked in 1% lead (II) acetate trihydrate (Pb(CH₃COO)₂ × 3H₂O, 467863, Sigma-Aldrich) and dried. The plate was shaken using an optical plate reader (Flex Station 3, Molecular Devices, Winnersh, UK) for 10 s and briefly centrifugated. The top of the well plate was covered with pre-made lead acetate-saturated filter paper and tightly sealed with a plastic lid. Subsequently, the assembly was incubated for 1 h at 37°C in a 5% CO₂ incubator. The filter paper was imaged using ChemiDoc[™] MP (Bio-Rad) using a colorimetric setting. The spot intensities were quantified from images using GeneTools[®], version 4.3.10.0 (Syngene, Cambridge, UK).

2.12 | Data analysis and statistics

Data were recorded in an electronic laboratory notebook eLABJOURNAL (Bio-ITech, Groningen, The Netherlands). Values in bar graphs are expressed as mean \pm SEM (standard error of the mean), *n* refers to the number of animals in each group. Unless otherwise specified, the differences between the groups were analyzed by either 2 way-ANOVA (for parametric data) followed by Tukey's multiple comparisons test or Kruskal-Wallis (for non-parametric data) followed by Dunn's method. Data analysis was performed using R version 4.0.2 and RStudio 1.3.1056. *p* values of less than .05 (two tailed) were considered statistically significant.

3 | RESULTS

3.1 | Flanking *Cbs* exon 3 with loxP sites does not produce negative effects

Schematic diagrams of the genetic constructs for establishing the inducible *Cbs*^{-/-} line are shown in Figure 1A. To

investigate potential leaky Cre-ERT2 expression with subsequent negative effects of the floxed *Cbs* allele during embryogenesis or early life, we used RT-qPCR followed by gel electrophoresis to determine the genotypes of all pups originating from *Cre-ERT2*^{+/-} *Cbs*^{fl/fl} × *Cre-ERT2*^{-/-} *Cbs*^{fl/fl} breeding pairs (Figure 1B). The average litter size was 9 \pm 2 (*n* = 13 litters). In these, the frequency of the *Cre-ERT2*^{+/-} genotype was exactly 50% (59 out of 118), indicating no adverse effects of the *Cre-ERT2*^{+/-} *Cbs*^{fl/fl} genotype before induction.

3.2 | Verification of genetic knockout of *Cbs*

All animals were treated with tamoxifen or vehicle (corn-oil) for 5 days at an average age of 10 weeks and were followed until 90 weeks of age. At termination, CBS expression in liver, kidney and brain was analyzed by Western blot analysis (Figure 2A). *Cbs*^{-/-} showed profound downregulation of CBS protein abundance in liver and kidney (1.01 \pm 0.03 and 9.9 \pm 2.2 AU in *Cbs*^{-/-} vs. 211 \pm 59 and 95 \pm 56 in *Cbs*^{fl/fl}, respectively), but not in brain (12.9 \pm 0.1 vs. 11 \pm 1.1 AU).

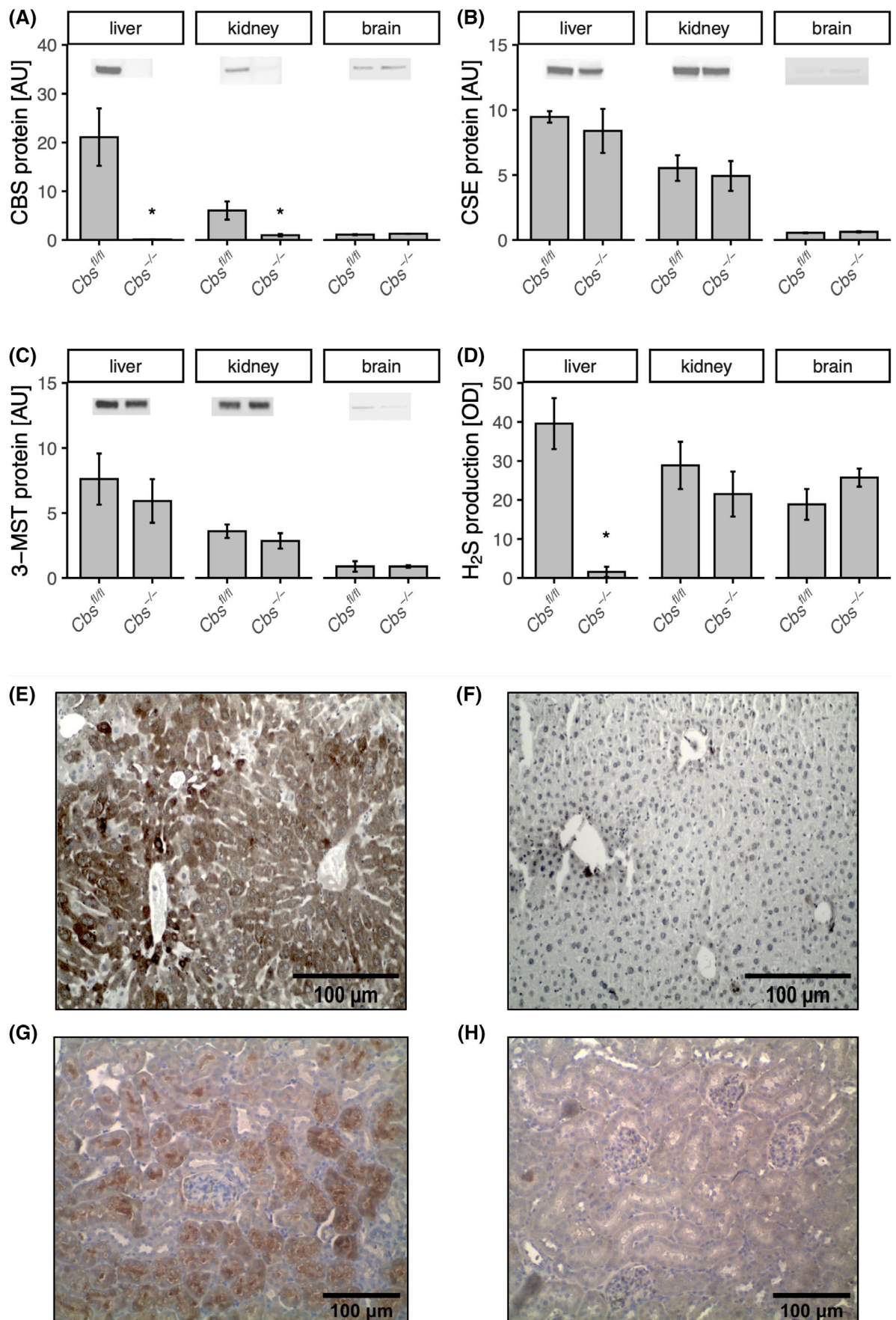
To investigate a potential compensatory upregulation of other hydrogen sulfide (H₂S) producing enzymes, we determined the expression of cystathionine gamma-lyase (CSE) and 3-mercapto- pyruvate sulfurtransferase (3-MST). CSE (Figure 2B) and 3-MST (Figure 2C) protein expression was highly expressed in liver, less in kidney and minimally in the brain with no differences between *Cbs*^{-/-} and *Cbs*^{fl/fl}.

H₂S production capacity was determined in organ lysates using an assay with the substrates homocysteine and cysteine (Figure 2D). CBS-mediated H₂S production was severely decreased in the liver of *Cbs*^{-/-} compared to *Cbs*^{fl/fl} (39 \pm 7 vs. 1.6 \pm 1.3 AU, respectively, *p* < .05). H₂S production in the kidney showed high variation and was not significantly decreased in *Cbs*^{-/-} compared to *Cbs*^{fl/fl} (11 \pm 4 vs. 17 \pm 13 AU, respectively, NS). *Cbs*^{-/-} did not affect H₂S production in the brain compared to *Cbs*^{fl/fl} (26 \pm 2 vs. 19 \pm 4 AU, respectively, NS).

Considering that protein expression of CBS was significantly down-regulated in *Cbs*^{-/-} liver and kidney but not in brain (Figure 2A), we proceeded to localize CBS expression by performing immunohistochemistry on formalin-fixed and paraffin-embedded tissue. In *Cbs*^{fl/fl}, strong CBS staining was observed throughout the liver and kidney (Figure 2E,G). In contrast, CBS staining was undetectable in *Cbs*^{-/-} liver and kidney (Figure 2F,H).

3.3 | Phenotypic characterization

In addition to the primary groups of tamoxifen and corn-oil treated homozygous *Cbs*^{fl/fl} *Cre-ERT2*^{+/-} (*Cbs*^{-/-} (*n*



= 10) and $Cbs^{fl/fl}$ ($n = 8$), respectively), we also included tamoxifen and corn-oil treated heterozygous $Cbs^{fl/+}$ $Cre-ERT2^{+/-}$ ($Cbs^{+/-}$ and Cbs^{+fl} , respectively, all $n = 8$) and tamoxifen and corn-oil treated $Cbs^{fl/fl}$ $Cre-ERT2^{-/-}$ ($Cbs^{fl/fl} + T$ and $Cbs^{fl/fl} + C$, respectively, all $n = 8$).

During the course of the study, all mortalities and terminations were registered, and autopsy was performed if needed. No significant differences in mortality were observed between groups (χ^2 test $p > .05$). One mouse in the $Cbs^{-/-}$ group was prematurely euthanized because of eye injury following retro-orbital blood sampling and one died of unknown reasons at the age of 54 weeks. In the $Cbs^{fl/fl}$ group, one mouse died from heat shock during blood pressure measurement and another mouse was humanely euthanized because of self-inflicted wounds from scratching (age 77 weeks). In the Cbs^{+fl} group, one mouse died immediately after corn-oil injection and one mouse died at the age of 41 weeks presumably as a result of a large abdominal cyst. In the $Cbs^{fl/fl} + C$ group, one animal died at the age of 85 weeks for unknown reasons. No deaths were observed in the $Cbs^{+/-}$ and $Cbs^{fl/fl} + T$ groups.

Prior to tamoxifen or corn-oil injections, absolute body weights were similar in all animal groups and this time point was used as baseline for normalization of body weight gain (Figure 3A). During the course until 90 weeks of age, $Cbs^{-/-}$ animals exhibited a lean habitus which was reflected by less growth (Figure 3A). Furthermore, body fat composition measured using magnetic resonance revealed that $Cbs^{-/-}$ mice had significantly ($p < .05$) less body fat (4.1 ± 1.1 g) compared to $Cbs^{fl/fl}$ (6.4 ± 2.3 g), whereas lean body weights did not differ (21.9 ± 1.1 g and 21.6 ± 2.3 g, respectively).

Alopecia was observed only in $Cbs^{-/-}$ mice (Figure 3B). The loss of hair was predominantly facial and became first noticeable approximately 4 months after knockout induction. The severity of alopecia increased over time, resulting in complete loss of facial hair, loss of whiskers and overall poor coat quality by the end of the study. Surprisingly, 3 out of 8 $Cbs^{-/-}$ mice did not develop substantial alopecia, despite severely raised homocysteine levels (296 ± 40 μ M $n = 3$, Figure S1A). Immunohistochemical staining of coronal (Figure 3C) and transverse (Figure 3E) skin sections in $Cbs^{fl/fl}$, showed presence of CBS in sebaceous glands and epidermis. In contrast, minimal CBS staining was observed in sebaceous glands and epidermis of $Cbs^{-/-}$ (Figure 3D,F) with lack of hair development in the bulb.

Furthermore, hair follicles appeared dilated with thinner epithelium in $Cbs^{-/-}$. Facial skin samples of $Cbs^{-/-}$ did not demonstrate abnormalities in the thickness of dermis, epidermis, or hypodermis (Figure S1B,C).

Investigation of mice in metabolic cages for 24 h at 80 weeks of age demonstrated higher water intake in $Cbs^{-/-}$ than in $Cbs^{fl/fl}$ (7.3 ± 0.5 g vs. 3.7 ± 1.0 g, respectively, Table 2). However, two-way ANOVA analysis on all groups indicated that this difference was related to tamoxifen treatment ($p < .01$) and not to genotype ($p = .14$). Urinary output did not differ between groups (Table 2).

Homocysteine was elevated in the plasma (tHCy, total plasma homocysteine) approximately 100-fold in $Cbs^{-/-}$ mice compared to mice from control the groups $Cbs^{fl/fl}$, Cbs^{+fl} , $Cbs^{fl/fl} + C$, $Cbs^{fl/fl} + T$ (289 μ M ± 58 vs. < 5 μ M, respectively), while $Cbs^{+/-}$ mice showed only a mild increase in tHCy (Table 2). Weights of heart, kidneys, spleen, liver, and brain were similar in all groups (Table 2). Mean arterial blood pressures were 90.2 ± 9.0 mmHg in $Cbs^{fl/fl}$ mice and 87.3 ± 14.8 mmHg in $Cbs^{-/-}$ mice, 10 weeks after tamoxifen injections. Hematological profiles were consistent across animal groups, with no statistically significant differences in the counts of platelets, white blood cells and red blood cells (RBC), in hemoglobin, hematocrit, or mean RBC corpuscular volume (MCV) (Table 2).

3.4 | CBS deficiency causes vascular endothelial dysfunction

To assess the effects of CBS deficiency on vascular function, thoracic aorta was preserved in cold saline solution, cut into rings, and mounted in a Mulvany myography setup. Endothelium-dependent relaxation (EDR) was measured in rings precontracted with phenylephrine (PE) with subsequent stimulation by acetylcholine (Figure 4A–C).

Acetylcholine-induced maximal relaxation was strongly impaired in $Cbs^{-/-}$ compared to $Cbs^{fl/fl}$ mice (E_{max} $44 \pm 28\%$ and $80 \pm 9\%$ respectively, $p < .001$, Figure 4A, areas under curves (AUC) $p < .001$, Figure 4D). In contrast, maximal EDR in the aorta of $Cbs^{+/-}$ and Cbs^{+fl} mice were not different (E_{max} $66 \pm 15\%$ and $57 \pm 17\%$ respectively, Figure 4B). $Cbs^{fl/fl} + T$ demonstrated decreased vasorelaxation upon cumulative stimulation with acetylcholine compared to $Cbs^{fl/fl} + C$ mice as reflected by their E_{max} ($58 \pm 22\%$ and 72

FIGURE 2 Verification of tamoxifen-induced Cbs knockout. (A–C) Expression of Cystathionine- β -synthase (CBS), Cystathionine- γ -lyase (CSE) and 3-mercaptopyruvate sulfurtransferase (3-MST) in major organs, respectively. (D) Production of hydrogen sulfide (H_2S) by organ lysates from cysteine and homocysteine was measured as lead sulfide precipitate on paper. Representative images of immunohistochemical staining of CBS (DAB, brown) in paraffin-embedded livers (E and F) and kidneys (G and H) were taken with 20 \times magnification and are shown for a $Cbs^{fl/fl}$ mouse, and $Cbs^{-/-}$ mouse, respectively. Hematoxylin was used to counterstain cell nuclei (blue). Data are shown as mean \pm SEM, with * representing $p < .05$ calculated using a Mann–Whitney test

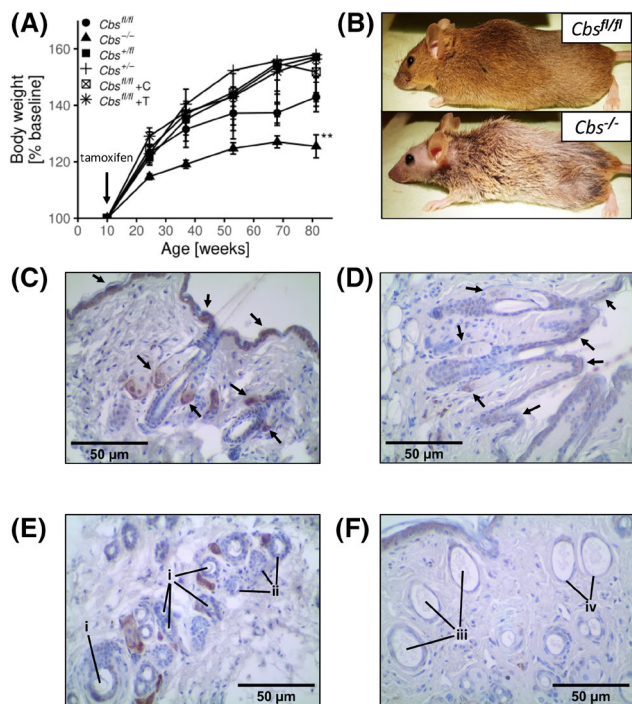


FIGURE 3 Inducible *Cbs* knockout leads to reduced body weight gain, facial alopecia, and poor hair condition caused by follicular dysfunction. (A) Body weight (BW) throughout the course of the study, expressed as percentage of baseline starting from induction with tamoxifen. (B) Representative photographs of hair condition of a *Cbs*^{fl/fl} control mouse and a tamoxifen-treated *Cbs*^{-/-} animal, depicting facial alopecia and poor coat quality. (C) Representative coronal sections of the scalp hair follicles from a *Cbs*^{fl/fl} control mouse with CBS staining (DAB, brown) and hematoxylin counterstain. Closed arrows point out positive CBS signal in the sebaceous glands and epidermis. (D) The absence of hair growth in the scalp of a *Cbs*^{-/-} mouse. Open arrows indicate low CBS expression in sebaceous glands. (E) Representative transverse sections of hair follicles (indicated with i) in the scalp of a *Cbs*^{fl/fl} mouse and normal epithelial thickness (indicated with ii). (F) In *Cbs*^{-/-} animals, follicles were enlarged and contained particulate matter (iii). The follicular epithelium was stretched and thin (iv). Data are shown as mean \pm SEM, with ** representing $p < .01$ for area under curve compared to *Cbs*^{fl/fl} mice calculated using a Mann-Whitney test

$\pm 5\%$ respectively, $p = .015$, Figure 4C) and AUC ($p = .03$, Figure 4D). Additionally, EDR was measured in the absence of nitric oxide (NO) production after preincubating aortic rings with the non-specific NOS inhibitor L-NMMA. *Cbs*^{-/-} aortas no longer relaxed as evidenced by an E_{\max} of $-5.5 \pm 11.5\%$ compared to *Cbs*^{fl/fl} ($E_{\max} = 13.7 \pm 25.2\%$, $p < .001$, Figure 4E). The contribution of NO to EDR was calculated as the difference between AUC of L-NMMA-preincubated relaxation and AUC of vehicle-preincubated relaxation. Aortas from *Cbs*^{-/-} demonstrated a significantly reduced NO-mediated EDR when compared to *Cbs*^{fl/fl} ($p = .047$, Figure 4F).

Contractile responses to KCl and PE were identical between groups (Figures S2A,B). Moreover, PE-mediated precontraction force after preincubation with $100 \mu\text{M}$ L-NMMA was not affected by CBS deficiency in aortas from *Cbs*^{-/-} mice (Figure S2C).

To exclude potential involvement of cGMP signaling in endothelial dysfunction, aortas were precontracted with PE and stimulated with sodium nitroprusside (SNP), a direct NO donor. *Cbs*^{-/-} and *Cbs*^{fl/fl} aortas exhibited identical endothelium-independent relaxation after preincubation with or without preincubation with L-NMMA (Figure S2D,E, respectively).

3.5 | Effect of CBS deficiency on markers of senescence and organ damage

Considering the role of CBS in redox homeostasis, we measured systemic oxidative load represented by plasma hydrogen peroxide (H_2O_2) at the ages of 40 and 80 weeks. At the age of 40 weeks, average H_2O_2 concentrations were significantly increased in plasma of *Cbs*^{-/-} over the plasma of *Cbs*^{fl/fl} mice ($89 \pm 4 \mu\text{M}$ and $70 \pm 9 \mu\text{M}$, respectively, $p < .05$, Figure 5A). At week 80, levels of H_2O_2 were found similar in all groups (Figure S3A).

Expression of manganese-dependent superoxide dismutase (*MnSOD*) mRNA in liver (Figure 5B) was found significantly upregulated in *Cbs*^{-/-} compared to *Cbs*^{fl/fl} controls (1.31 ± 0.09 vs. 0.96 ± 0.12 AU, respectively, $p < .05$). In addition, we investigated a panel of senescence-associated markers expressed in liver. The expression of tumor suppressor factor p53, the pro-inflammatory cytokines *IL-6* and *IL-1b* did not significantly differ between groups (Figure S3B–D). Potential liver damage was further assessed by measuring plasma alanine aminotransferase (ALAT), showing similar levels in *Cbs*^{-/-} compared to other groups (Figure S3E).

Given the age of the animals and the potential involvement of CBS in aging processes, we additionally screened a panel of senescence markers in the liver. The mRNA expression of tumor suppressor *p16* and Lamin B1 (LMNB1) were significantly upregulated in *Cbs*^{-/-} compared to *Cbs*^{fl/fl} (Figure 5C,D). A similar trend was observed for p21, but this did not reach statistical significance (Figure S3F). Regucalcin, also known as Senescence Marker Protein-30 (SMP-30) did not differ between groups (Figure S3G).

Kidney dysfunction was explored by assessing albumin-creatinine ratio in urine (ACR) at the age of 36 weeks. ACR of *Cbs*^{-/-} showed a slight increase compared to *Cbs*^{fl/fl}, however this difference was statistically insignificant (Figure S3H). Consistently, HE-stained kidneys showed no signs of tubular necrosis or degeneration,

TABLE 2 Animal characteristics and clinical presentation

Group	<i>Cbs^{fl/fl}</i>	<i>Cbs^{-/-}</i>	<i>Cbs^{+/fl}</i>	<i>Cbs^{+/-}</i>	<i>Cbs^{fl/fl} + C</i>	<i>Cbs^{fl/fl} + T</i>
N	7	6	6	8	8	8
tHCy (μ M)	4.9	289.6 (58.3) ^{d***}	3.1	7.6	3.6	4.2
Body Weight (g)	32.7 (4.1)	31.7 (2.3)	36.5 (3.9)	41.0 (8.5)	39.5 (3.4)	34.5 (3.7)
Heart (mg)	241.2 (65.3)	226.0 (52.7)	235.0 (48.1)	228.0 (49.7)	245.5 (26.9)	206.0 (46.8)
Left kidney (mg)	233.2 (78.7)	244.7 (43.0)	263.0 (73.5)	239.9 (57.1)	265.2 (65.2)	232.8 (29.8)
Right kidney (mg)	233.7 (80.5)	267.2 (45.2)	285.5 (98.3)	238.1 (57.2)	275.5 (61.3)	256.2 (37.4)
Spleen (mg)	134.0 (102.9)	142.2 (159.0)	59.0 (1.4)	157.6 (139.9)	154.8 (83.9)	172.3 (155.6)
Liver (mg)	1347.7 (265.3)	1673.8 (359.5)	1575.5 (163.3)	2081.6 (423.9)	1996.0 (408.9)	2401.0 (2264.2)
Brain (mg)	491.8 (32.8)	469.2 (36.4)	497.0 (18.4)	481.3 (53.7)	520.8 (42.2)	495.8 (52.7)
Water intake (g)	4.16 (1.61)	6.87 (0.72) ^{b**}	3.73 (0.99)	7.33 (0.49) ^{c***}	5.29 (1.93)	7.26 (0.48) ^{a*}
Urine output (g)	0.74 (0.61)	0.63 (0.38)	0.96 (0.78)	1.16 (0.54)	1.05 (0.87)	1.25 (1.19)
WBC ($10^3/\mu$ l)	5.04 (4.17)	8.25 (5.25)	5.45 (1.91)	4.91 (1.73)	4.91 (2.11)	3.56 (1.36)
RBC ($10^6/\mu$ l)	9.42 (1.10)	9.12 (1.28)	10.5 (2.64)	12.7 (1.96)	11.0 (1.62)	11.9 (2.01)
HGB (g/dl)	8.32 (0.89)	7.83 (1.66)	8.98 (2.06)	10.7 (1.21)	9.16 (1.20)	10.1 (1.67)
HCT (%)	0.48 (0.05)	0.46 (0.09)	0.52 (0.13)	0.63 (0.07)	0.52 (0.07)	0.60 (0.11)
MCV (fl/cell)	50.6 (0.80)	49.6 (4.24)	49.6 (0.90)	49.9 (2.22)	48.7 (1.32)	50.3 (3.21)
Platelets ($10^3/\mu$ l)	1306 (1945)	2069 (901)	1630 (1354)	1214 (516)	1753 (663)	1268 (687)

Note: Values are shown as mean (SD). Total plasma homocysteine (tHCy) was measured in pooled samples from each group; hence no SD were calculated. Comparisons for statistical inference: groups *Cbs^{fl/fl} + C* and *Cbs^{fl/fl} + T*: a, groups *Cbs^{fl/fl}* and *Cbs^{-/-}*: b, groups *Cbs^{+/fl}* and *Cbs^{+/-}*: c, groups *Cbs^{-/-}* and *Cbs^{+/-}*: d.

Abbreviations: HCT, hematocrit; HGB, hemoglobin; MAP, Mean arterial pressure; MCV, mean corpuscular volume; RBC, red blood cells; WBC, white blood cells.

* $p < .05$; ** $p < .01$; *** $p < .001$.

no loss of brush border and glomeruli did not display sclerosis (Figure S4).

Given that HHCy is suggested to induce non-alcoholic steatohepatitis (NASH),³⁰ we next investigated liver lipid deposition using ORO staining. Despite strongly increased HHCy levels, *Cbs^{-/-}* genotype did not lead to changes in liver lipid deposition (Figure S5A–C). Similarly, periodic acid-Schiff staining did not reveal significant differences in glycogen abundance (Figure S5D–F). In livers stained with hematoxylin and eosin (HE), no differences in steatosis scores were observed between study groups (Figure S5D). Fibrosis was not present in any of the investigated tissue sections. Evaluation of H&E-stained liver using SAF (Steatosis, Activity and Fibrosis) scoring suggested ballooning and lobular inflammation in *Cbs^{-/-}* mice (Figure S5G,H,I). While *Cbs^{+/-}* mice demonstrated a similar SAF score compared to *Cbs^{fl/fl} + C* and *Cbs^{fl/fl} + T* mice, significantly lower SAF score was observed in livers of *Cbs^{+/fl}* mice (Figure S5G).

4 | DISCUSSION

CBS is an enzyme that plays a central role in HHCy by limiting the rate of homocysteine clearance from plasma.

To study the effects of CBS and subsequent HHCy on a pathological level, it is crucial to establish a reliable and robust *Cbs* knockout model. Our findings demonstrate the successful development and characterization of a Cre-inducible *Cbs^{-/-}* mouse. Mice demonstrated no perinatal mortality and were followed until 90 weeks of age. Despite severe HHCy, *Cbs^{-/-}* showed a mild phenotype with impaired weight gain, alopecia, endothelial dysfunction, but no increased mortality nor signs of liver or kidney damage.

The tamoxifen-induced *Cbs^{-/-}* model developed in this study introduces several advantages over previously reported *Cbs* knockout models. First, non-induced mice developed normally without perinatal mortality as demonstrated by the expected Mendelian distribution of genotypes in the offspring. This is in stark contrast to the initial CBS deficiency mouse model by Watanabe et al.,¹⁶ that exhibit severe hepatic fibrosis, hepatomegaly and liver failure, resulting in high neonatal mortality. Moreover, our model does not depend on the expression of transgenic human CBS to reduce neonatal mortality, such as the Tg-I278T model.^{15,20,31} As the transgene is driven by a zinc-inducible metallothionein promoter, its expression and regulation across various tissues likely differs from that of endogenous CBS, implying that the

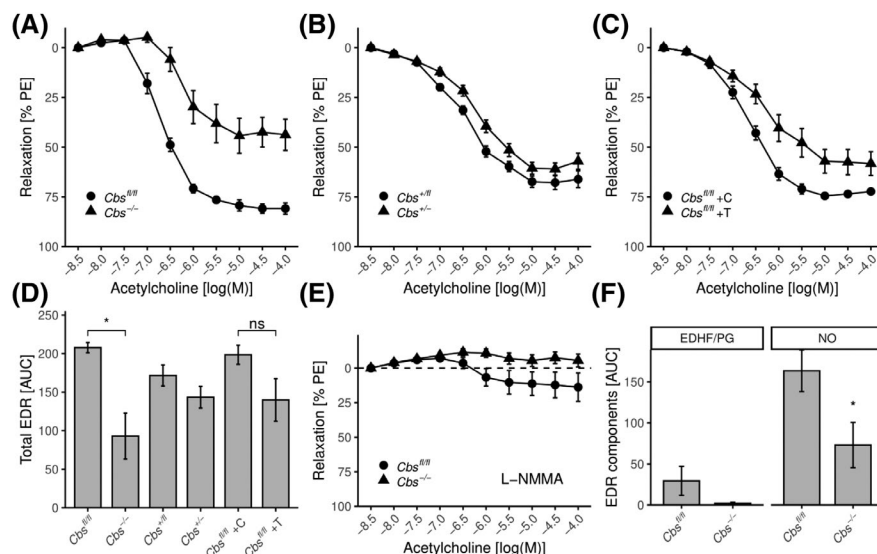


FIGURE 4 CBS deficient mice develop endothelial dysfunction. (A–C) Endothelium-dependent relaxation responses (EDR) of thoracic aortic rings to acetylcholine after 20 min pre-incubation with vehicle control and pre-constriction with 1 μ M phenylephrine (PE). (D) Acetylcholine-induced EDR from panels A–C expressed as area under curve (AUC). EDR was dramatically decreased in *Cbs*^{-/-} mice when compared to *Cbs*^{+/+} controls. Although with lower magnitude, tamoxifen treatment also decreased total EDR in *Cbs*^{+/+} + T mice when compared to *Cbs*^{+/+} + C controls. (E) Acetylcholine-induced relaxation responses were also measured after inhibition of NO production with L-NMMA, and were absent in *Cbs*^{-/-} mice, and almost completely abolished in the *Cbs*^{+/+} group. The absence of relaxation after inhibition with L-NMMA indicates that endothelium-derived hyperpolarization factor (EDHF) and prostaglandins did not participate in relaxation, and that EDR was predominantly mediated by NO. (F) Contribution of the NO component to EDR expressed as AUC and calculated as a difference between curves from panels A and E. Data in bar graphs are expressed as mean \pm SEM. Group means were compared using the Mann–Whitney test, depicted with * p < .05, *** p < .001

results obtained with these models may not reflect the natural role of CBS. Finally, our model does not require zinc-sulphate in drinking water to maintain transgene expression. Administration of zinc sulphate introduces potentially toxic effects,³² including increased consumption of glutathione in the process of sulphate metabolism.³³

Aside from the advantages that the tamoxifen-induced Cre/LoxP *Cbs*^{-/-} model may have over other models, some key aspects remain in common. First, the HHCy is severe ($298 \pm 58 \mu$ M) and similar to that of the Tg-I278T model (298μ M). Second, our model also presented impaired weight gain soon after induction. Both the Tg-I278T and the Cre/LoxP *Cbs*^{-/-} mouse models were induced at comparable ages (30–40 days and 63 days, respectively) and did not show biochemical or histological evidence of severe damage in the liver or kidney.^{26,34} Though histological SAF scoring of *Cbs*^{-/-} livers suggested ballooning and inflammation, this was not confirmed by biochemical analysis. Moreover, these findings challenge the HHCy ‘threshold’ theory, which presupposes a buffering mechanism which fails to protect if HHCy exceeds 169μ M.²⁰ Rather, our study shows that severe HHCy alone does not drive damage in liver and kidney in *Cbs* knockout mice.

In this study, alopecia or loss of facial hair in *Cbs*^{-/-} mice was in accord with previous studies of *Cbs* deficient mice.^{35–37} However, the skin layers of Tg-I278T CBS-deficient mice were previously reported to thin in comparison to control mice,²⁶ whereas in the present study we found that epidermis, dermis, and hypodermis were of the same thickness in *Cbs*^{-/-} and *Cbs*^{+/+} mice. At present, the reason for these differences are unclear. In the Tg-I278T model, the mutated human CBS gene is driven by a metallothionein-I promoter (mMT-I) during gestation. As mMT-I is highly expressed in epidermal keratinocytes,³⁸ it may be possible that supraphysiological expression of the CBS transgene in keratinocytes in the Tg-I278T model may have resulted in disturbed skin development. Alternatively, dermal CBS expression in our tamoxifen-induced *Cbs*^{-/-} model may not have been completely blocked, which may have resulted in normal skin thickness. Taken together, our data demonstrate that the observed alopecia is not directly related to skin thickness. Nevertheless, we established several morphological changes in the scalp of *Cbs*^{-/-} mice. In particular, we observed thinning of the follicular epithelium and enlargement of hair follicles that did not contain hair, suggesting that the alopecia is caused by disturbed follicular integrity.

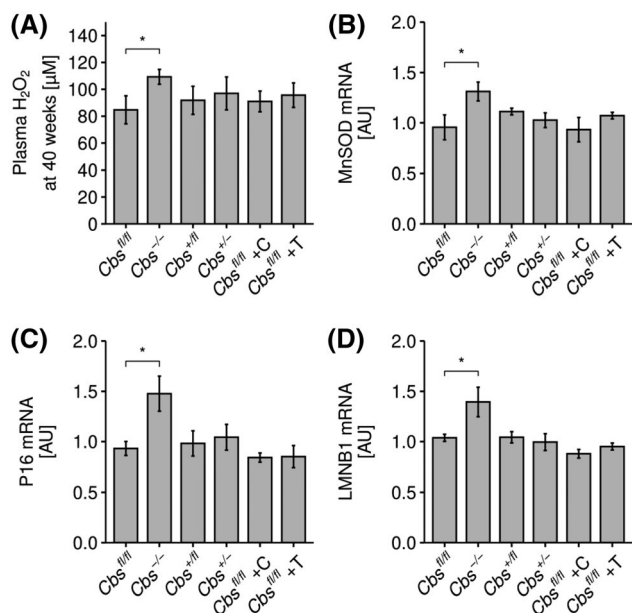


FIGURE 5 Inducible knockout of *Cbs* promotes systemic ROS formation and senescence. (A) Plasma hydrogen peroxide H₂O₂ concentration measured 30 weeks after administration of tamoxifen. (B) Liver mRNA expression of mitochondrial manganese superoxide dismutase. (C) Liver expression of the senescence markers P16, (D) and lamin B1. Data are shown as mean ± SEM of molar concentration or arbitrary units (AU), with * representing $p < .05$ calculated using a Mann–Whitney test

Although it is not fully understood why CBS-deficient mice develop alopecia, previous studies managed to prevent or partially reverse facial alopecia in *Cbs* knockout mice by methionine-restricted diet, systemic administration of CBS, and liver-specific gene therapy.^{26,36,37} These results suggest that systemic metabolic disturbances might be the cause of facial alopecia rather than local CBS deficiency. Surprisingly, not all *Cbs*^{-/-} mice developed alopecia in our study, despite severely elevated plasma homocysteine levels in all mice. Moreover, plasma homocysteine levels did not correlate with the severity of alopecia. These results suggest that local factors may contribute to alopecia. We therefore investigated local CBS expression in skin and found CBS expression at the base of the sebaceous glands and in the epidermis, with considerably lower presence of CBS in *Cbs*^{-/-} mice. Interestingly, some previous studies showed that sebaceous glands play an important role in the pathophysiology of alopecia by the means of dysregulated lipogenesis, dysfunctional disintegration of sebocytes, and atrophy.^{39–41} The localization of CBS in the sebaceous gland could therefore hint towards a contributing role of CBS in the pathophysiology of sebaceous glands in alopecia, supporting our hypothesis that alopecia is primarily a follicular problem. Future studies may resolve this issue by determining dermal homocysteine, hydrogen sulfide and CBS expression levels in relation to the severity of alopecia.

Increased oxidative load is a common feature of HHCy.⁴² Indeed, in our study *Cbs*^{-/-} mice had elevated plasma levels of hydrogen peroxide compared to *Cbs*^{fl/fl} at 40 weeks of age. However, at the time of termination at 80 weeks of age, levels of ROS were further elevated, but there was no longer a significant difference between the groups. Further evidence of pro-oxidative status in *Cbs*^{-/-} was found in the liver, namely the increased expression of MnSOD, a mitochondrial antioxidant enzyme that converts superoxide radicals, a major by-product of mitochondrial respiration, into hydrogen peroxide.

In the present study, we observed endothelial dysfunction in *Cbs*^{-/-} mouse aorta, which was characterized by impaired NO-mediated relaxation. Considering that sensitivity of the vascular smooth muscle to NO was unaltered, endothelial dysfunction was rooted either in underproduction of NO, or in quenching by ROS, as superoxides are known to reduce the bioavailability of NO.⁴³ Our findings closely parallel previous studies using mouse small mesenteric arteries and aortas^{7,24} in which the knockout of *Cbs* increased endothelial superoxide production causing endothelial dysfunction. Even though the product of CBS, H₂S, is known to be part of a complex of factors collectively known as Endothelium-Derived Hyperpolarizing Factor or EDHF, we ruled out its importance in aortic relaxation in the present model. Arguably, the contribution of EDHF to the relaxation of a conduit artery such as the aorta is typically small, in contrast to peripheral resistance arteries.⁴⁴ Moreover, the predominant source of H₂S in the vasculature is cystathionine-γ-lyase (CSE),¹¹ suggesting that the endothelial dysfunction observed in our study was not a direct consequence of CBS knockout in the endothelium.

Recent findings in a rat model of HHCy revealed evidence of accelerated aging represented by upregulation of p16, p21 and p53 in vascular smooth muscle cells.⁴⁵ Accelerated aging was reflected in our study as well, particularly in the increase of liver mRNA of the senescence associated markers p16, IL-1b, but not p21 nor p53. Surprisingly, the senescence marker Lamin B1 was found upregulated, whereas in senescence it is typically found downregulated.⁴⁶ However, a recent study suggested that Lamin B1 upregulation may also be a marker of increased oxidative stress.⁴⁷

Although the tamoxifen-induced Cre/LoxP *Cbs*^{-/-} model has significant advantages over other models, several limitations should be considered. First, the induction with tamoxifen may affect liver and vascular function. To address this potential issue, we investigated the effects of tamoxifen in control *Cbs*^{fl/fl} mice lacking the Cre-ERT2 transgene and excluded harmful or confounding effects of tamoxifen. Second, previous studies suggested that the knocking *in* and knocking *out* of H₂S producing enzymes

could exert a compensatory effect on other H₂S producing enzymes, CSE and 3-MST.⁴⁸ This point was also addressed in the present study, and we found no evidence of compensatory overexpression of CSE and 3-MST in the kidney or liver that would support this claim. Finally, the possibility that complete genetic deletion of *Cbs* was not achieved in all tissues and organs was studied. This was most apparent in the brain of *Cbs*^{-/-} mice, where CBS expression was not affected by tamoxifen induction. This observation may be related to low expression of the Cre-ERT2 transgene in the brain.⁴⁹

5 | CONCLUSION

In conclusion, *Cbs*^{fl/fl} mice developed normally until tamoxifen induction of Cre-ERT2, resulting in effective *Cbs*^{-/-} and CBS deficiency in the liver, skin, and kidney, but not in brain. Phenotypically, mice demonstrated severe HHCy, facial alopecia, endothelial dysfunction, increased oxidative stress, and more abundant markers of senescence. Despite severe HHCy, *Cbs*^{-/-} mice did not show signs of liver or kidney damage, in contrast to previous mouse models which employed transgenic human CBS enzymes. CBS expression in the skin localized to sebaceous glands and the epidermis, suggesting a site-specific effect of CBS deficiency in the development of alopecia.

5.1 | Innovation

The Cre-ERT2 *Cbs*^{fl/fl} mice have normal levels and localization of CBS expression before induction, and therefore provide a considerable improvement for studying the role of endogenous CBS in (patho)physiology over transgenic crippled CBS models. Our model demonstrated no signs of liver and kidney damage despite severe HHCy, indicating that HHCy alone is not the driver for the development of end-organ damage. Moreover, our data contributes to a growing field of evidence that CBS is important for hair maintenance, particularly in relation to the observed alopecia and the role of the sebaceous gland herein.

ACKNOWLEDGEMENTS

The authors wish to thank Dr. Floris Fojer for providing Cre-ERT2 mice, and to acknowledge Dr. Jojanneke J Bruintjes for providing several of the genetic constructs used to generate the *Cbs* knockout mice.

DISCLOSURES

The authors declare no conflict of interest.

AUTHOR CONTRIBUTIONS

R. H. Henning, L. E. Deelman, J. H. Buikema, and B. van de Sluis conceived the idea, designed experiments, and directed work. D. Nakladal, S. P. H. Lambooy, R. H. Henning and L. E. Deelman co-wrote the manuscript, analyzed data, prepared figures, and contributed to discussion. A. van Buiten, M. Goris, N. J. Kloosterhuis, N. Huijkman, L. E. Deelman, R. H. Henning and D. Nakladal performed animal experimental work. D. Nakladal, S. P. H. Lambooy, S. Mišúth, D. Čepcová, C. P. Joschko, and F. Hoogstra-Berends performed molecular analyses. G. F. Diercks consulted and reviewed dermatological assessments. All authors reviewed the manuscript.

DATA AVAILABILITY STATEMENT

The data that support the findings of this study are available in the results, methods and/or Supporting Information of this article.

ORCID

D. Nakladal  <https://orcid.org/0000-0003-0900-0130>

REFERENCES

1. Boushey CJ, Beresford SA, Omenn GS, Motulsky AG. A quantitative assessment of plasma homocysteine as a risk factor for vascular disease. Probable benefits of increasing folic acid intakes. *JAMA*. 1995;274:1049-1057.
2. Ganguly P, Alam SF. Role of homocysteine in the development of cardiovascular disease. *Nutr J*. 2015;14:6.
3. Karmin O, Siow YL. Metabolic imbalance of homocysteine and hydrogen sulfide in kidney disease. *Curr Med Chem*. 2018;25:367-377.
4. Beyer K, Lao JI, Carrato C, et al. Cystathionine beta synthase as a risk factor for Alzheimer disease. *Curr Alzheimer Res*. 2004;1:127-133.
5. Son P, Lewis L. *Hyperhomocysteinemia*. StatPearls (StatPearls Publishing); 2021.
6. Kim C-S, Kim Y-R, Naqvi A, et al. Homocysteine promotes human endothelial cell dysfunction via site-specific epigenetic regulation of p66shc. *Cardiovasc Res*. 2011;92:466-475.
7. Jiang X, Yang F, Tan H, et al. Hyperhomocysteinemia impairs endothelial function and eNOS activity via PKC activation. *Arterioscler Thromb Vasc Biol*. 2005;25:2515-2521.
8. Kang SS, Wong PW, Malinow MR. Hyperhomocyst(e)inemia as a risk factor for occlusive vascular disease. *Annu Rev Nutr*. 1992;12:279-298.
9. Zaric BL, Obradovic M, Bajic V, et al. Homocysteine and hyperhomocysteinemia. *Curr Med Chem*. 2019;26:2948-2961.
10. Weber Hoss GR, Sperb-Ludwig F, Schwartz IVD, Blom HJ. Classical homocystinuria: a common inborn error of metabolism? An epidemiological study based on genetic databases. *Mol Genet Genomic Med*. 2020;8:e1214.
11. Kanagy NL, Szabo C, Papapetropoulos A. Vascular biology of hydrogen sulfide. *Am J Physiol Cell Physiol*. 2017;312:C537-C549.
12. Hine C, Zhu Y, Hollenberg AN, Mitchell JR. Dietary and endocrine regulation of endogenous hydrogen sulfide

- production: implications for longevity. *Antioxid Redox Signal*. 2018;28:1483-1502.
13. Wu D, Gao B, Li M, et al. Hydrogen sulfide mitigates kidney injury in high fat diet-induced obese mice. *Oxid Med Cell Longev*. 2016;2016:2715718.
 14. Polhemus DJ, Li Z, Pattillo CB, et al. A novel hydrogen sulfide prodrug, SG1002, promotes hydrogen sulfide and nitric oxide bioavailability in heart failure patients. *Cardiovasc Ther*. 2015;33:216-226.
 15. Arndt S, Baeza-Garza CD, Logan A, et al. Assessment of H₂S in vivo using the newly developed mitochondria-targeted mass spectrometry probe MitoA. *J Biol Chem*. 2017;292:7761-7773.
 16. Watanabe M, Osada J, Aratani Y, et al. Mice deficient in cystathionine beta-synthase: animal models for mild and severe homocyst(e)inemia. *Proc Natl Acad Sci U S A*. 1995;92:1585-1589.
 17. Park I, Hůlková H, Krijt J, et al. Long-term uninterrupted enzyme replacement therapy prevents liver disease in murine model of severe homocystinuria. *Hum Mutat*. 2020;41:1662-1670.
 18. Robert K, Nehmé J, Bourdon E, et al. Cystathionine beta synthase deficiency promotes oxidative stress, fibrosis, and steatosis in mice liver. *Gastroenterology*. 2005;128:1405-1415.
 19. Akahoshi N, Kobayashi C, Ishizaki Y, et al. Genetic background conversion ameliorates semi-lethality and permits behavioral analyses in cystathionine β -synthase-deficient mice, an animal model for hyperhomocysteinemia. *Hum Mol Genet*. 2008;17:1994-2005.
 20. Gupta S, Kühnisch J, Mustafa A, et al. Mouse models of cystathionine beta-synthase deficiency reveal significant threshold effects of hyperhomocysteinemia. *FASEB J*. 2009;23:883-893.
 21. Maclean KN, Sikora J, Kožich V, et al. A novel transgenic mouse model of CBS-deficient homocystinuria does not incur hepatic steatosis or fibrosis and exhibits a hypercoagulable phenotype that is ameliorated by betaine treatment. *Mol Genet Metab*. 2010;101:153-162.
 22. Brenton DP, Dow CJ, James JJ, Hay RL, Wynne-Davies R. Homocystinuria and Marfan's syndrome. A comparison. *J Bone Joint Surg Br*. 1972;54:277-298.
 23. Gupta S, Kruger WD. Cystathionine beta-synthase deficiency causes fat loss in mice. *PLoS One*. 2011;6(11):e27598.
 24. Cheng Z, Jiang X, Kruger WD, et al. Hyperhomocysteinemia impairs endothelium-derived hyperpolarizing factor-mediated vasorelaxation in transgenic cystathionine beta synthase-deficient mice. *Blood*. 2011;118:1998-2006.
 25. Dayal S, Chauhan AK, Jensen M, et al. Paradoxical absence of a prothrombotic phenotype in a mouse model of severe hyperhomocysteinemia. *Blood*. 2012;119:3176-3183.
 26. Gupta S, Melnyk SB, Kruger WD. Cystathionine β -synthase-deficient mice thrive on a low-methionine diet. *FASEB J*. 2014;28:781-790.
 27. Quentin R, Pierre F, Dubois M, Soutoul JH, Goudeau A. Frequent isolation of capnophilic bacteria in aspirate from Bartholin's gland abscesses and cysts. *Eur J Clin Microbiol Infect Dis*. 1990;9:138-141.
 28. Ventura A, Kirsch DG, McLaughlin ME, et al. Restoration of p53 function leads to tumour regression in vivo. *Nature*. 2007;445:661-665.
 29. Speir RW, Stallings JD, Andrews JM, et al. Effects of valproic acid and dexamethasone administration on early bio-markers and gene expression profile in acute kidney ischemia-reperfusion injury in the rat. *PLoS One*. 2015;10:e0126622.
 30. Dai Y, Zhu J, Meng D, Yu C, Li Y. Association of homocysteine level with biopsy-proven non-alcoholic fatty liver disease: a meta-analysis. *J Clin Biochem Nutr*. 2016;58:76-83.
 31. Wang L, Jhee KH, Hua X, DiBello PM, Jacobsen DW, Kruger WD. Modulation of cystathionine beta-synthase level regulates total serum homocysteine in mice. *Circ Res*. 2004;94:1318-1324.
 32. Fosmire GJ. Zinc toxicity. *Am J Clin Nutr*. 1990;51:225-227.
 33. Leustek T. Sulfate metabolism. *Arabidopsis Book*. 2002;1:e0017.
 34. Gupta S, Wang L, Slifker MJ, et al. Analysis of differential neonatal lethality in cystathionine β -synthase deficient mouse models using metabolic profiling. *FASEB J*. 2021;35:e21629.
 35. Robert K, Maurin N, Ledru A, Delabar J, Janel N. Hyperkeratosis in cystathionine beta synthase-deficient mice: an animal model of hyperhomocysteinemia. *Anat Rec*. 2004;280A:1072-1076.
 36. Majtan T, Jones W, Krijt J, et al. Enzyme replacement therapy ameliorates multiple symptoms of murine homocystinuria. *Mol Ther*. 2018;26:834-844.
 37. Lee H-O, Salami CO, Sondhi D, et al. Long-term functional correction of cystathionine β -synthase deficiency in mice by adeno-associated viral gene therapy. *J Inherit Metab Dis*. 2021;44:1382-1392.
 38. Hanada K, Sawamura D, Hashimoto I, Kida K, Naganuma A. Epidermal proliferation of the skin in metallothionein-null mice. *J Invest Dermatol*. 1998;110:259-262.
 39. Rittié L, Tejasvi T, Harms PW, et al. Sebaceous gland atrophy in psoriasis: an explanation for psoriatic alopecia? *J Invest Dermatol*. 2016;136:1792-1800.
 40. Sundberg JP, Shen T, Fiehn O, et al. Sebaceous gland abnormalities in fatty acyl CoA reductase 2 (Far2) null mice result in primary cicatricial alopecia. *PLoS One*. 2018;13:e0205775.
 41. Whiting DA. Cicatricial alopecia: clinico-pathological findings and treatment. *Clin Dermatol*. 2001;19:211-225.
 42. Zou C-G, Banerjee R. Homocysteine and redox signaling. *Antioxid Redox Signal*. 2005;7:547-559.
 43. Fukai T, Ushio-Fukai M. Superoxide dismutases: role in redox signaling, vascular function, and diseases. *Antioxid Redox Signal*. 2011;15:1583-1606.
 44. Jiang J, Zheng J-P, Li Y, et al. Differential contribution of endothelium-derived relaxing factors to vascular reactivity in conduit and resistance arteries from normotensive and hypertensive rats. *Clin Exp Hypertens*. 2016;38:393-398.
 45. Yan W, Cao Y, Zhen P, et al. Decreased autophagy of vascular smooth muscle cells was involved in hyperhomocysteinemia-induced vascular ageing. *Clin Exp Pharmacol Physiol*. 2021;48:524-533.
 46. Freund A, Laberge R-M, Demaria M, Campisi J. Lamin B1 loss is a senescence-associated biomarker. *Mol Biol Cell*. 2012;23:2066-2075.
 47. Chen X, Zhao X, Cai H, et al. The role of sodium hydrosulfide in attenuating the aging process via PI3K/AKT and CaMKK β /AMPK pathways. *Redox Biol*. 2017;12:987-1003.
 48. Li N, Wang MJ, Jin S, et al. The H₂S donor NaHS changes the expression pattern of H₂S-producing enzymes after myocardial infarction. *Oxidative Med Cell Longev*. 2016;2016:1-11.

49. Hameyer D, Loonstra A, Eshkind L, et al. Toxicity of ligand-dependent Cre recombinases and generation of a conditional Cre deleter mouse allowing mosaic recombination in peripheral tissues. *Physiol Genomics*. 2007;31:32-41.

SUPPORTING INFORMATION

Additional supporting information may be found in the online version of the article at the publisher's website.

How to cite this article: Nakladal D, Lambooy SPH, Mišúth S, et al. Homozygous whole body *Cbs* knockout in adult mice features minimal pathology during ageing despite severe homocysteinemia. *FASEB J*. 2022;36:e22260. doi:[10.1096/fj.202101550R](https://doi.org/10.1096/fj.202101550R)